Eng. Sci., 2020, 10, 58–67

Engineered Science

DOI: https://dx.doi.org/10.30919/es8d1003

Temperature Dependent Studies on Radio Frequency Sputtered Al Doped ZnO Thin Films

Pankaj K. Bhujbal, Habib M. Pathan and Nandu B. Chaure*

Abstract

In this work, highly conductive and transparent Al: ZnO (Al doped ZnO, i. e., AZO) thin films were grown by radio frequency (RF) magnetron sputtering technique at a typical deposition temperature. The effect of deposition temperature on the structural, morphological, optical and electrical properties was studied. The x-ray diffraction (XRD) studies revealed a hexagonal wurtzite crystal structure for all AZO layers with a (002) preferred orientation along the c-axis. Columnar, compact, uniform grain growth of the layer was observed from atomic force microscopy (AFM) images. The deposition temperature had an influence on the surface roughness and average grain size of deposited films, which could be confirmed by means of AFM images. Optical studies confirmed that both optical band gap energy and urbach energy were influenced by the substrate temperature. Highly transparent films with an energy band gap ranging from 3.48 to 3.65 eV were obtained upon changing the deposition temperature from 22 to 400℃. The presence of defects was confirmed by photoluminescence (PL) spectra. A systematic measurement of the electrical parameters like barrier height, and ideality factor of the devices (Ag/Al:ZnO) was carried out with the help of *I-V* characteristic. This study may be useful for the design and fabrication of AZO based electrodes for solar cell applications.

Keywords: Al:ZnO; RF magnetron sputtering; Urbach energy; Ideality factor; Deposition temperature
Received: 30 January 2020; Accepted: 7 March 2020
Article type: Research article

1. Introduction

Transparent conducting oxides (TCOs) have numerous applications in optoelectronics and electronic devices like light emitting diodes (LEDs), flexible electronic devices, flat panel displays, solar cells,[1-3] sensors,[4-6] *etc*. Indium tin oxide (ITO) is one of the most commonly used TCOs, however, the toxicity, limited availability and high cost of the indium are major issues. Therefore, the prime concern is to find an alternative to the ITO material.

Al doped zinc oxide (Al:ZnO, i.e., AZO) is the most promoting alternative because of its environmental stability and transparency. ZnO is a n-type semiconductor with a wide band gap. Pristine ZnO shows low and unstable electrical properties, like conductivity and mobility. Doping with some transition metals can modify the properties of ZnO thin films. For example, group III elements like Ba,[7] Al,[8] Ga[7, 9] and In[7] are deposited into ZnO, which allows to achieve both high optical transparency and high conductivity. Among the III group elements, Al is commonly used to improve the properties of pristine ZnO, i. e., transparency, stability, and conductivity. AZO thin films have gained much interest due to their large exciton binding energy (60 meV) at 22℃, wide optical energy band gap (3.37 eV) and high chemical stability.[10] Along with a high optical transparency in the visible range, AZO films have superior electrical conductivity, good thermal and chemical stability.[11]

Numerous methods and techniques have been reported to deposit AZO films like chemical vapor deposition (CVD),[12] RF magnetron sputtering,[11,13,14,15] sol-gel method,[16] spray pyrolysis,[17-19] and pulsed laser deposition.[20-23] RF magnetron sputtering is one of the promising methods for the deposition of AZO films because it offers film deposition at lower temperatures as well as a better adhesion than other methods. It is popularly used in industry because its parameters can be easily controlled, the films can be obtained with a high packing density and strong adhesions at a relatively high deposition rate.[24] The physical such as electrical properties of AZO films are influenced by various deposition parameters like Al_2O_3 content in the target,

Department of Physics, Savitribai Phule Pune University, (formerly University of Pune) Pune 411007, India
** **E-mail:** n.chaure@physics.unipune.ac.in*

deposition time, RF power, Ar gas pressure, and deposition temperature.[25] Thus, it is important to study the effects of the deposition parameter on the deposition of the AZO films. Deposition temperature is one of the most significant parameters as it can tune electrical, optical and structural properties.

In order to study various electrical parameters like barrier height, ideality factor, saturation current, *etc*, Ohmic and Schottky contacts are normally made. For AZO, it is more difficult to fabricate rectifying or Schottky contacts than Ohmic contacts. The reasons can be the diffusion of metal into the semiconductor, chemical reactions between metal and semiconductor and the defects in the surface region.[26-27] Schottky contacts are mostly used in many applications like the stand-alone photovoltaic systems, power supply, *etc*. Many researchers found that n-ZnO along with Au, Ag, and Pd (low-reactive metals) can form comparatively high Schottky barriers.[28-30] For example, Ozgur *et al*. reported that to make the Schottky barrier, a high work function metal has to be applied to the surface of a ZnO.[27,31] The thermal stability of Au/n-ZnO Schottky junction has not been studied. It has reported that at high temperatures (>330K), Au based contacts have some serious issues like the degradation of samples with the thermal cycling and their poor I-V characteristics.[29,30,32,33] Simpson *et al*.[34] found that the thermal stability of the Au/ n- ZnO based Schottky contact was lower than that of Ag based Schottky contact. In 2002, Sheng *et al*.[35] developed the Ag/ZnO Schottky diode, studied its electrical characteristics and reported the electrical parameters like ideality factor and barrier height as 1.33 and 0.89 eV. Keskenler *et al*.[27] fabricated an Ag/n-ZnO/p-Si/Al heterojunction diode by the sol-gel spin coating technique and found the barrier height and ideality factor of 0.71 and 2.03 eV, respectively. In 2013, Dondapati *et al*.[36] investigated the optical as well as plasmonic properties of AZO thin films for various substrate temperatures to understand the fundamentals of carrier generation and transport characteristics. Aliasghar *et al*.[37] prepared AZO film by DC-magnetron sputtering and found that the band-gap energy and urbach energy of AZO film was 3.2 and 0.4 eV, respectively. They also calculated the barrier height and ideality factor to be about 10 and 0.3 eV, respectively for Au/Al: ZnO devices. Pathirane *et al*.[38] reported the AZO/Ag nanowire (NW) electrodes for solar cells with Ag NW coated on the AZO. However, the barrier height and ideality factor for this particular device were not reported.

Herein, the AZO films were grown by RF magnetron sputtering and the effects of substrate temperature on the microstructural, morphological, optical and electrical properties were investigated and the relations between them were established. The carrier generation and current transport mechanisms of AZO films were also studied. The optical behavior of AZO films along with urbach energy and band gap energy was described as well. In order to study the electrical measurement, the Ag contacts on the AZO film were made by using the thermal evaporation technique.

2. Experimental

2.1 AZO thin film preparation

An AZO film was grown by the RF magnetron sputtering onto a microscopic glass substrate. The substrates were cleaned in acetone and ethanol by using an ultrasonic cleaning. Fig. 1A shows a schematic diagram of the RF magnetron sputtering system, which was used to grow AZO thin films.

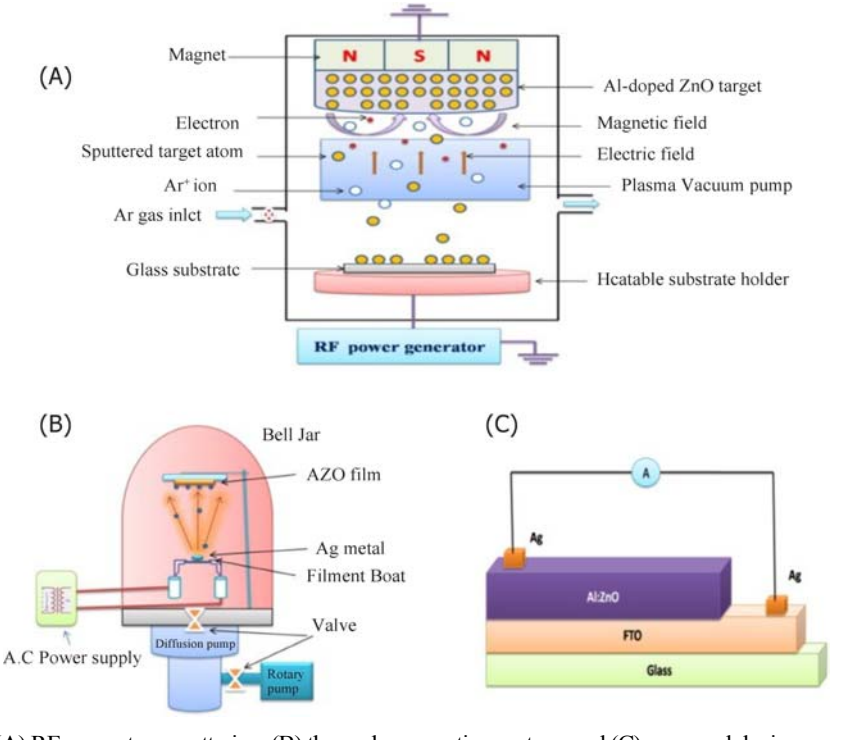

Fig. 1 Schematic diagram of (A) RF magnetron sputtering, (B) thermal evaporation system, and (C) proposed device, used for electrical measurements.

The AZO target with a Cu bonding (99.99% purity, Al: ZnO = 2:98 wt%) was procured from Testbourne Ltd. UK. The turbo molecular pump was used to evacuate the sputtering chamber at a base pressure lower than 10_{-4} torr. The flow rate of Ar (80 sccm) was controlled by a mass flow controller. The RF power was set at a constant 200 W. The AZO film depositions were carried out in the temperature range from 22 to 400℃ for 15 minutes for all samples. Table 1 shows the parameters used for the deposition of AZO film.

Table 1. The parameters used for the deposition of AZO film.

Parameter	Number
Target	AZO
Thickness of the target (mm)	3
Diameter of the target (mm)	76.2
Weight ratio of Al to ZnO	2 : 98
Chamber base pressure (torr)	< 10-4
Ar flow rate (cm^3/min)	80
RF power (W)	200
Deposition time (min)	15
Temperature (℃)	22-400

2.2 Fabrication of Device (Ag / Al:ZnO)

Fig. 1C shows the fabricated Al /Al:ZnO device for the present study. For the fabrication of proposed device, the Ag metal contacts were made on the top surface of AZO films by thermal evaporation technique, (Fig. 1B). In the present systematic study, the effects of deposition temperature on the microstructural, morphological, optical andelectrical properties of Ag /Al: ZnO junction were investigatedby the thermionic emission theory.

2.3. Characterizations

The physical properties, microstructures, morphologies, optical properties and electrical properties of the AZO thin films were studied systematically under the influence of deposition temperatures. The optical band gap, specular transmittance, urbach energy and absorption were carried out by JASCOV-670 UV-Vis spectrophotometer. The electronic structures and defect related transitions of AZO films were studied using a Perkin Elmer LS-55 photoluminescence spectrometer. The film thicknesses were obtained from the fringes observed in the transmission spectra using Swanepole's calculations. The structural properties of the AZO films were performed to investigate the crystallinity, crystallite size and crystal orientation of the deposited films using X-ray diffractometer, model Bruker D8 with Cu K_{α} radiation having a wavelength of 0.154nm. The atomic force microscopy (AFM) was used to study the surface morphology. The DC electrical measurements, i. e. ideality factor, saturation current, barrier height, electrical conductivity and resistivity of the deposited AZO films, were carried out by MODEL 4200-SCS Semiconductor Characterization System and four-probe measurement unit.

3. Results and discussion

3.1 X-ray diffraction (XRD)

Fig. 2 shows the typical XRD pattern of AZO films deposited at different deposition temperatures. Fig. 3 shows the magnified part of the XRD patterns for the detailed study of (004) diffraction peaks. The AZO films were grown at 22 to 400℃. All films show the peak at about 34°, corresponding to the (002) reflection of hexagonal wurtzite crystal structure (JCPDS card No 36-1451).[11,39,40] It has been observed that the (002) and (004) diffraction peak intensity increases with increasing the deposition temperature up to 300℃ due to the enhancement in the crystallinity of AZO films. This enhancement may be related to the increases of atomic mobility and surface diffusion of the adsorbed species, the reduction of structural defects, and the increased size of the grains. With the additional increase in the deposition temperature, the intensity of (002) and (004) peak was found to be decreased and an additional peak (101) appeared around 72.5°. This could be associated with the decreased crystallinity at a higher temperature (such as 400 ℃), which is attributed to the stress and lattice mismatch[13,41] between the surface of microscopic glass substrate and AZO layer.

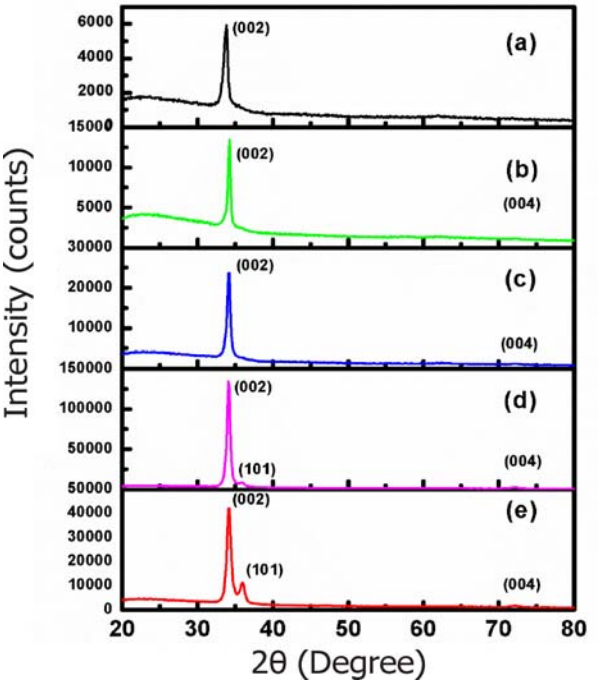

Fig. 2 XRD patterns of AZO films deposited at (a) 22, (b) 100, (c) 200, (d) 300 and (e) 400℃.

Debye formula was used to determine the average crystallite size (d) of AZO films by using Equation (1):

$$d = \frac{0.9\lambda}{\beta \cos\theta} \quad (1)$$

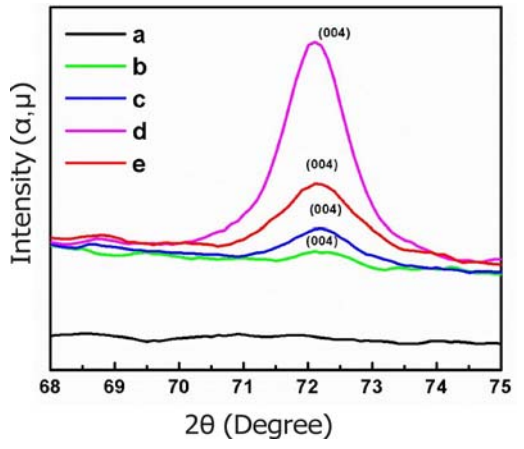

Fig. 3 Magnified XRD spectra of AZO films deposited at (a) 22, (b) 100, (c) 200, (d) 300 and (e) 400℃.

where θ, β and λ are the Bragg diffraction angle, a full-width at half maximum (FWHM) of the diffraction peak, and the wavelength of the used x-ray. Fig. 4 shows the graph plotted for the crystallite size and FWHM versus substrate temperature. It shows that the films grown at 100 and 300℃ have a high crystallite size and less FWHM. The parameters like microstrain (ε) and dislocation (δ) density were calculated by using Equations 2 and 3, respectively.[11,13,43]

$$\varepsilon = \beta \cos\frac{\theta}{4} \quad (2)$$

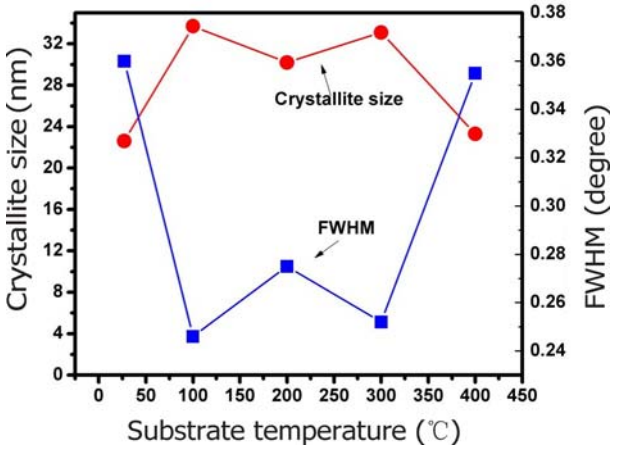

Fig. 4 Crystallite size and FWHM vs. deposition temperature of AZO films deposited at (a) 22, (b) 100, (c) 200, (d) 300 and (e) 400℃.

and

$$\delta = 1/(d)^2 \quad (3)$$

The calculated data of those films are summarized in Table 2. It shows that the dislocation density of AZO films grown at 100 and 300℃ is low, which is attributed to the reduced crystal lattice due to the imperfections and crystal defects produced at high temperatures. The present XRD study revealed that the films grown at 100 and 300℃ show a good crystallinity as well as a large particle size.

3.2. Surface morphology

The deposited AZO films were characterized by atomic force microscopy (AFM) to identify the surface roughness and other surface-related parameters. Fig. 5A and B represents the 3D AFM images of AZO films deposited at 200 and 300℃, respectively. The average grain size of AZO films was determined by AFM images at different substrate temperatures. Both films have a columnar structure, attributed to the c-axis crystallite orientation along the substrate.[40,11] It is also revealed that the surface related parameters of AZO films are influenced by the substrate temperature. Upon increasing the deposition temperature, the grain size was found to be increased, which could be associated with the agglomeration of smaller size grains. The agglomeration of grains is responsible for the high mobility of particles that gives larger sized structures.[44] This result is well consistent with the XRD result.

Table 2. Estimated FWHM, crystallite size, microstrain and dislocation density from XRD data.

Deposition temperature (℃)	FWHM (Degree)	Crystallite size (nm)	Microstrain	Dislocation density (cm^{-2})
22	0.360	22.6	0.0062	1.90×10^{11}
100	0.246	33.7	0.0043	0.87×10^{11}
200	0.275	30.2	0.0047	1.09×10^{11}
300	0.252	33.1	0.0043	0.90×10^{11}
400	0.355	23.3	0.0062	1.80×10^{11}

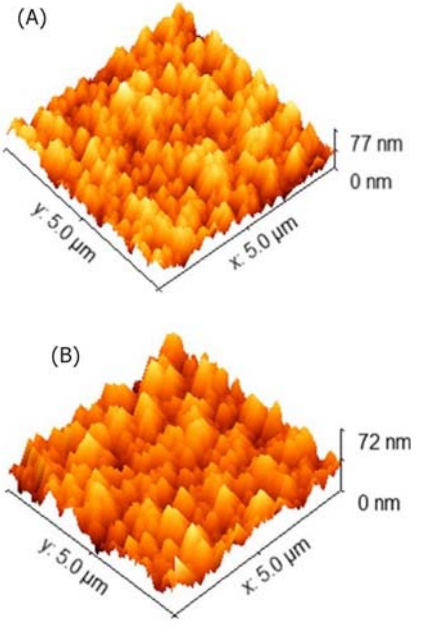

Fig. 5 AFM images (3D) of the AZO films grown at a deposition temperature of (A) 200 and (B) 300℃.

The average roughness, root mean square (RMS) roughness and average height of those films were also measured. The results are listed in Table 3. From AFM data, the average surface roughness increases with an increase in the deposition temperature. This is attributed to the increased

grain size.[45] The AFM results show that the quality of the film is influence by the substrate temperature.

Table 3. Morphological parameters of AZO films deposited at a deposition temperature of (a) 200 and (b) 300℃.

Deposition temperature (℃)	Average roughness (nm)	RMS roughness (nm)	Average height (nm)
200	6.67	8.33	30.29
300	8.15	9.95	30.31

3.3. UV-visible spectroscopy analysis

The optical parameters like band gap energy, urbach energy, optical absorption, and optical transmittance were studied using the UV-Vis spectroscopy. Fig. 6 shows the transmission spectra of AZO films deposited at various deposition temperatures (from 22 to 400℃). All the deposited films show a maximum transmission above 93% at 600 nm in the visible region. It is also shown that the transparency of the film is decreased with an increase of the deposition temperature at 550-800 nm wavelengths. Since at high temperatures, the average roughness of the sample is higher; hence, the optical scattering is more, leading to a less transparency.[44] This result is in good consistency with the AFM results. The transmittance is almost zero at the wavelength of 300-350 nm, which is related to the onset of fundamental absorption, this represents the Blue shift phenomenon (i. e. the absorption edge was shifted toward a shorter wavelength with an increase in the deposition temperature). It is attributed to the Burstein-Moss shift effect.[46] The following Equation (4) was used to calculate the Burstein-Moss shift,

$$E_F - E_{CB} = \left(\frac{h^2}{8m^*}\right)(3\pi^2 n)^{2/3} \quad (4)$$

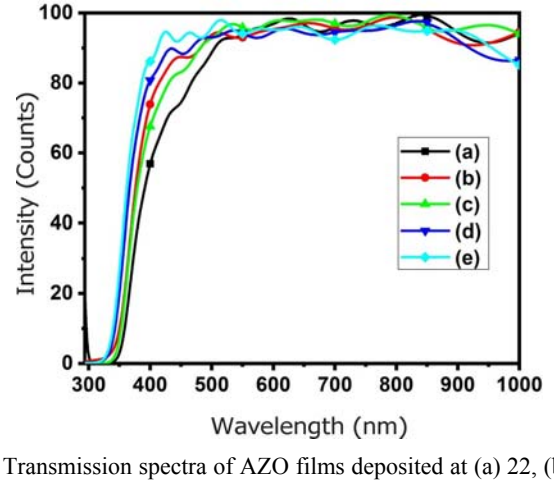

Fig. 6 Transmission spectra of AZO films deposited at (a) 22, (b) 100, (c) 200, (d) 300 and (e) 400℃.

where E_F, E_{CB}, n, and m^* are the Fermi level, conduction-band edge, carrier concentration and electron effective mass, respectively.[47,48] The energy band gap (E_g) was calculated by using the Tauc plot Fig. 7. The linearity in Tauc plot confirmed that the AZO has a direct transition type of the semiconductors.[49] The calculated energy band gaps are summarized in Table 4. It shows that as the deposition temperature increases, the optical band gap energy increases from 3.45 to 3.65 eV, attributed to the increase of structural order-disorders in the sample, which leads to a reduction of the intermediate energy levels and thus results in the accordingly progressing of the energy band gap.[50]

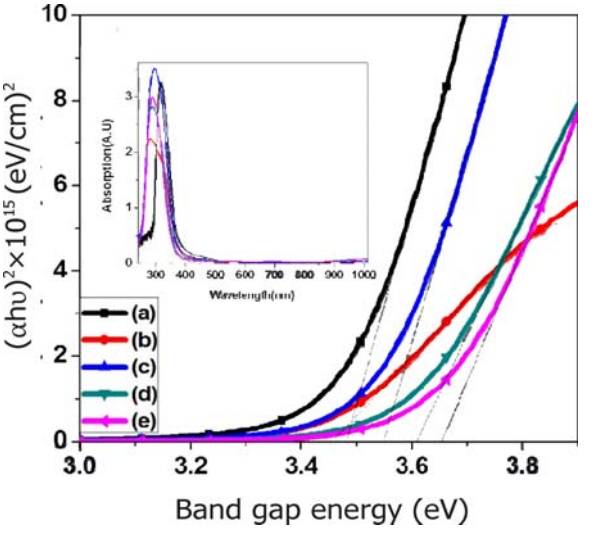

Fig. 7 The Tauc plot, inset absorption spectra of the AZO films grown (a) 22, (b) 100, (c) 200, (d) 300 and (e) 400℃, respectively.

Table 4. Variation of optical band gap and urbach energy of AZO films with temperature.

Deposition temperature (℃)	Band gap energy (eV)	Urbach energy (eV)
22	3.48	0.330
100	3.45	0.319
200	3.55	0.303
300	3.59	0.307
400	3.65	0.285

Urbach energy was calculated by taking the reciprocal of the slope of the natural logarithm of the absorption coefficient with wavelength. Fig. 8 shows the graphical representation of In(α) versus wavelength of AZO films grown at (a) 22, (b) 100, (c) 200, (d) 300 and (e) 400℃. The measured values are summarized in Table 4. The calculated values of urbach energy (E_u) was found to be less than the band gap energy of the AZO films. According to Sumi-Toyozawa (ST) model theory, the E_u is always less than the band gap energy, hence, the ST model theory can be well applied for this system.[51] According to researchers, the relation between urbach energy and band gap energy is inversely proportional.[50,52] In current investigation, an inverse relation is found between urbach and band gap energy. The absorption coefficient (α) below the optical band gap (tail absorption) depends exponentially on the

photon energy ($h\upsilon$) and can be represented in Equation (5):

$$\alpha = \beta \exp\left(\frac{h}{E_u}\right) \quad (5)$$

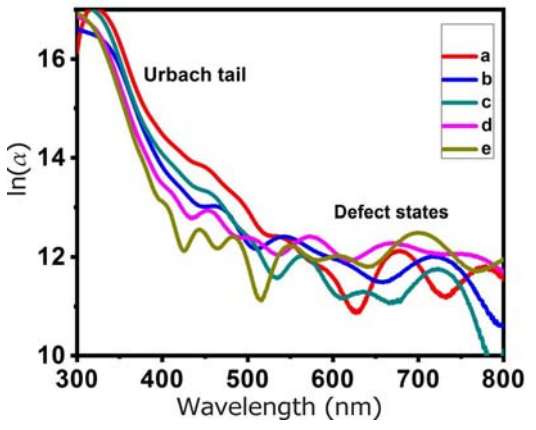

Fig. 8 Graphical representation of ln(α) vs. wavelength of AZO films grown at (a) 22, (b) 100, (c) 200, (d) 300 and (e) 400 ℃.

where β is constant, E is Urbach energy, h is plank constant, and is frequency.[53] Urbach energy strongly depends on the temperature, average photon energies, induced disorder, lattice thermal vibrations, static disorder, strong ionic bonds, *etc*.[50,54] From the above study, we found that as the temperature increases, the urbach energy decreases. Fig. 9 shows the graphical representations of temperature dependent band gap energy and urbach energy.

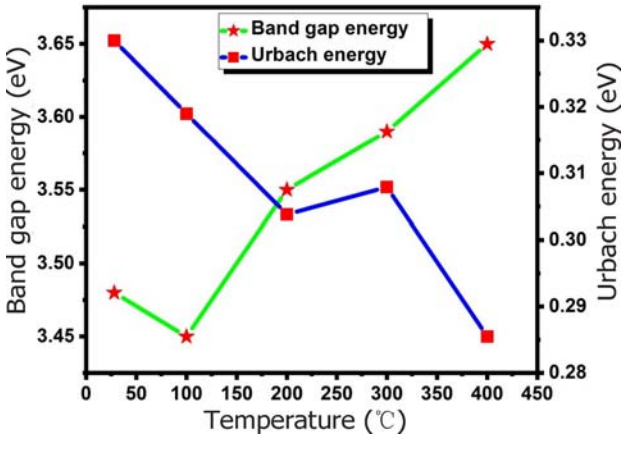

Fig. 9 Graphical representations of temperature dependent band gap energy and urbach energy.

The thickness of AZO films was calculated from the optical transmission spectra, using Swanepoel's calculations. The calculated thicknesses of corresponding films are summarized in Table 5. The above study shows that the film deposited at 300℃ has a high thickness compared to other films attributed to the increase in crystallite size and the enhancement in crystalline quality.[55] This result is in good consistence with the XRD and transmissions results.

3.4. Photoluminescence study

The photoluminescence (PL) spectra were used to determine the electronic structures and defect-related transitions at 295 K. In the present study, the influence of deposition temperature on the optical properties of the AZO films was studied. The PL intensity of AZO film was very sensitive to the defects and surface condition. Both defects and surface conditions were caused by the Al atoms, which were substituted with zinc atoms or occupied by interstitial sites. Fig. 10A shows the steady-state PL spectra of AZO films at an excitation wavelength of 325 nm. The UV emission transition peak (T_1) at 399 nm is related to the transition from near band edge to valance band.[11,56,57] The intensity of PL peak increases and the FWHM decreases with a rise in the film thickness, which are due to the enhancement in the crystallinity of the sample.[55] The film deposited at 300℃ showed the highest PL intensity due to a higher thickness and a higher crystallinity as compared with other films. The PL spectra exhibit deep level emission (DLE) peaks in the visible range, representing the emission of impurity or crystal defects,[58-60] like violet emission, violet-blue emission, blue emission, and green emission. The emission peak transition (T_2) around 418 nm is observed in all the AZO films, which is related to violet emission and attributed to the interstitial zinc (Zn_i) in the interface traps at the grain boundaries of the AZO films.[27] The emission peak (T) is related to the existing Zn_i defects in the AZO films. The emission peak (T_3) at around 447 nm is considered as the violet-blue emission arising from the oxygen (V_o) vacancies,[58] attributed to a transition from donor level of oxygen vacancy (V_o) to the valance band.[39] The emission peak (T_4) observed at 478 nm is related to the singlyionized oxygen vacancies (v_o) because of the transitions from $Zn \rightarrow V_{Zn}$.[13] The emission transition at 536 nm is responsible for green emission, because the trap electrons at the singly ionized oxygen vacancy are recombined with the photogenerated holes present in the valance band.[39,57] The schematic representation of all the transitions is represented in the energy level diagram, Fig. 10B.

Table 5. The calculated film thickness of the Al doped ZnO films deposited at a substrate temperature of (a) 22, (b) 100, (c) 200, (d) 300 and (e) 400℃.

Deposition temperature (℃)	Thickness (nm)
22	510
100	529
200	691
300	1352
400	1229

3.5 Electrical Properties

There are many important parameters like series resistance (R), ideality factor (n), saturation current (I_s), and barrier height (ϕ_b), which were estimated at 22℃ for the Ag/Al:

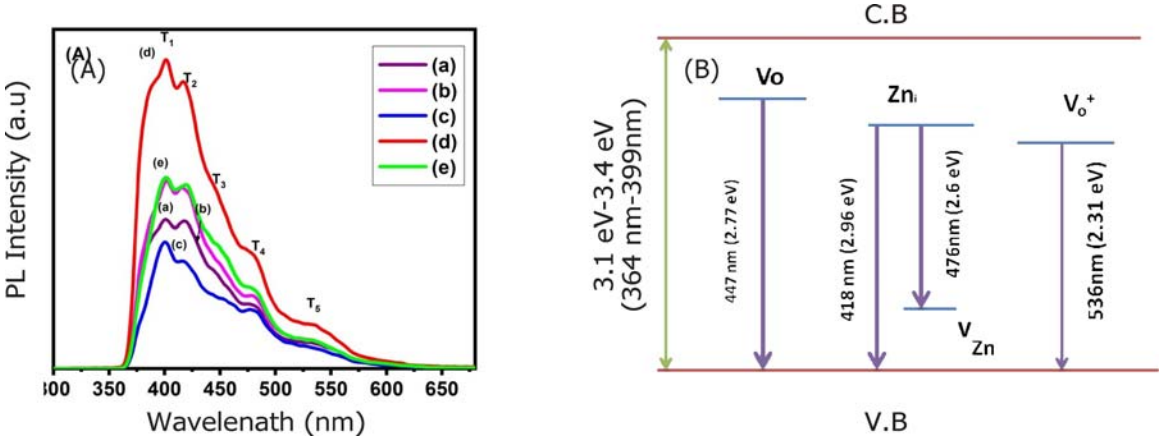

Fig. 10 (A) The photoluminescence (PL) spectra of the AZO films deposited at a deposition temperature of (a) 22, (b) 100, (c) 200, (d) 300 and (e) 400 ℃; and (B) Schematics of energy level diagram of an AZO film.

ZnO device to observe its electrical behaviour. The thermionic emission theory was applied to calculate those parameters, where n and ϕ_b are assumed to be independent of the voltage. The thermionic emission relation is given by following Equation (6),

$$I = \left[AA^*T^2 \exp\left(-\frac{q\varphi^b}{kT}\right)\right]\left[\exp\left(\frac{qV}{\eta kT}\right)-1\right] \quad (6)$$

where A is area of the sample, q is the charge on electron, ϕ_b is the effective barrier height, V is the applied voltage, A^* is the effective Richardson constant (for ZnO, A^* = 32 A $cm^{-2}K^{-2}$), n is the ideality factor, T is the absolute temperature, and k is the Boltzmann constant.[61] Equation 6 can be rewritten as Equation (7) by assuming $\frac{qV}{\eta kT} 1$,

$$I = I_s\left[\exp\left(\frac{qV}{\eta kT}\right)\right] \quad (7)$$

Here, I_s is the saturation current given by Equation (8):[62-64]

$$I_s = AA^*T^2 \exp\left(-\frac{q\varphi^b}{kT}\right) \quad (8)$$

Fig. 11 shows the *I-V* characteristic of the AZO films indicating a typical Schottky contact behavior for the Ag/Al: ZnO structure at 22℃. It provides the information about the electrical transport mechanisms, metal and semiconductor contact behavior and various electrical parameters of the proposed device. The ideality factor was calculated for the films grown at different substrate temperatures from the slope of ln(I) versus voltage (V) using Equation (9). Fig. 12 shows the plot of ln (I) versus applied voltage (V) of AZO films deposited at different deposition temperatures.

$$\eta = (q/kT)\mathrm{d}V/\mathrm{d}\ln(I) \quad (9)$$

where η is the ideality factor, k is Boltzmann constant, q is electron charge, and dV/dln(I) is the inverse of slope of ln(I) *vs*. V plot.[63] The calculated values are summarized in Table 5. The measured value of ideality factor is more than unity, which can be due to the barrier in the homogeneities of the sample. The deviation from the ideal value (i. e. one) may also be due to the presence of defects, interfacial states between metal and semiconductor, and current transport mechanisms except thermionic emission (generation/recombination in the depletion region and carrier tunneling through the barrier).[65,66] The barrier height of the device can be calculated by using the Schottky-Mott model.

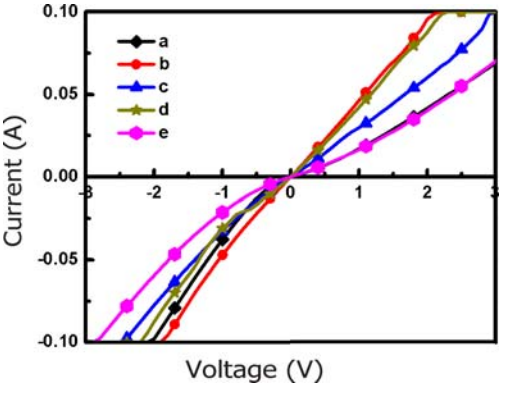

Fig. 11 *I-V* characteristic of the Ag/Al:ZnO configuration of AZO films deposited at a deposition temperature of (a) 22, (b) 100, (c) 200, (d) 300 and (e) 400℃.

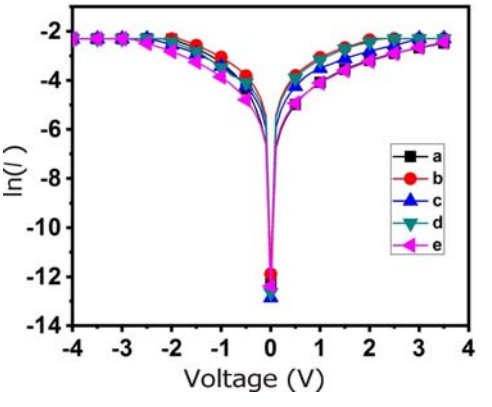

Fig. 12 Plot of ln(I) versus applied voltage (V) of AZO films de posited at a deposition temperature of (a) 22, (b) 100, (c) 200, (d) 300 and (e) 400℃.

The experimentally calculated values of barrier height and the ideality factor for the samples grown at different substrate temperatures are summarized in Table 6. Fig. 13 shows the graph of ideality factor and barrier height of the Ag contacted AZO films as a function of substrate temperature. The barrier heights were nearly consistent. The decreased value of ideality factor upon increasing the substrate temperature is the evidence of a reduction in the defects in the material and the formation of homogeneous AZO thin films.

Table 6. Measured electrical parameters for the films grown at different temperatures.

Deposition temperature (°C)	Ideality factor	Barrier height (eV)
22	4.05	0.318
100	3.78	0.317
200	3.56	0.322
300	3.54	0.331
400	4.01	0.321

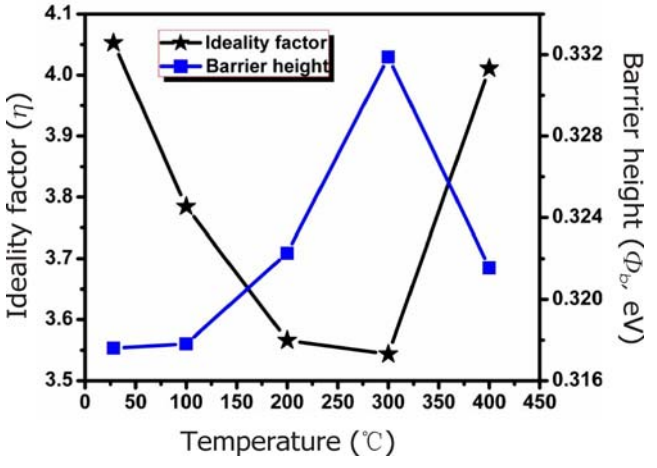

Fig. 13 Effect of deposition temperature on ideality factor and barrier height of Ag contacted AZO films at various deposition temperatures.

The influence of deposition temperature on the electrical property like resistivity of the AZO thin films is show in Fig. 14. The resistivity of deposited films declines with an increase in the deposition temperature up to 300℃, attributed to the rise in the oxygen defect. These defects acted as electron donors and the temperature directly affected the crystal quality and grain size of the films, which decreased the grain boundary scattering. The enhancement in the conductivity of AZO film is due to a better crystallinity. It improves the mobility of the AZO films by reducing the scattering of the carriers at the grain boundaries.[67] The film grown at 300℃ shows the lowest resistivity, i. e. 4.52×10^{-5} Ω m. However, with a further increase in the temperature, the resistivity of the film slightly increases because of an increased scattering in the grain boundaries and the deterioration of crystallinity.[68] This result is in good consistency with the XRD and AFM results.

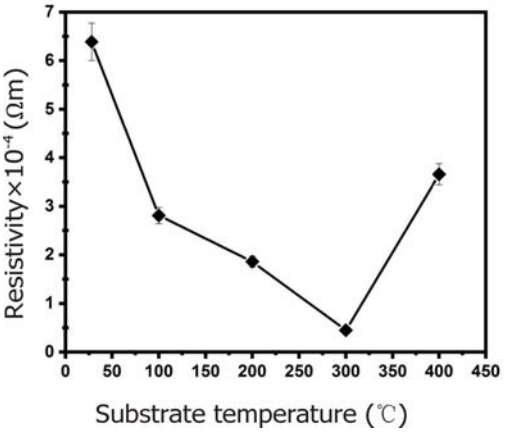

Fig. 14 Resistivity of the AZO films grown under various deposition temperatures.

4. Conclusions

In the present study, highly conducting and transparent AZO thin films were successfully grown by RF magnetron sputtering. A crystal growth of the AZO film was easily controlled by the depositing temperature. XRD analysis revealed that the deposited AZO film corresponded to the hexagonal wurtzite crystal structure and the size of crystallite increased as the deposition temperature increased. The AFM result revealed that all the films had a columnar crystal structure, i.e. the crystallite orientation along the c-axis (perpendicular to the glass substrate). It had been cleared from the AFM images that the average roughness of AZO films increased with increasing the deposition temperature. The energy band gap could be easily tuned by varying the deposition temperature. A PL spectrum clearly showed that the defect related transitions were present in the AZO films. The conductivity of AZO got enhanced by increasing the deposition temperature, one of the reasons might be the reduced scattering in the grain boundaries. The film grown at a deposition temperature of 300℃ acquired the lowest resistivity, i.e. 4.52×10^{-5} Ωm as well as a greater transparency (i.e. greater than 93% in the visible range). The electrical parameters like ideality factor and barrier height were measured for all the deposited films by assuming the thermionic emission model of the Schottky diode. Based on the current study, the AZO based material will be a promising electrode for future solar cell applications.

Acknowledgements

The authors acknowledge the Department of Science and Technology, Government of India for financial support vide Sanction order DST/TMD/SERI/S173 (G).

Notes

The authors declare no competing financial interest.

Supporting information
Not applicable

Conflict of interest
There are no conflicts to declare.

References

[1] M. Murugesan, D. Arjunraj, J. Mayandi, V. Venkatachalapathy and J. M. Pearce, *Mater. Lett.*, 2018, **222**, 50-53.

[2] M. Asemi, M. Ahmadi and M. Ghanaatshoar, *Ceram. Int*, 2018, **44**, 12862-12868.

[3] E. Aydin and N. D. Sankir, *Thin Solid Films*, 2018, **653**, 29-36.

[4] B. Nasr, S. Dasgupta, D. Wang, N. Mechau, R. Kruk and H. Hahn, *J. Appl. Phys*, 2010, **108**, 103721.

[5] Z. A. Wang, J. B. Chu, H. B. Zhu, Z. Sun, Y. W. Chen and S. M. Huang, *Solid. State. Electron*, 2009, **53**, 1149-1153.

[6] W. Beyer, J. Hüpkes and H. Stiebig, *Thin Solid Films*, 2007, **516**, 147-154.

[7] M. Tadatsugu, S. Hirotoshi, N. Hidehito and T. Shinzo, *Jpn. J. Appl. Phys.*, 1985, **24**, 10.

[8] J. Hong, H. Paik, H. Hwang, S. Lee, A. J. de Mello and K. No, *Phys. Status Solidi (a)*, 2009, **206**, 697-703.

[9] G. K. Paul and S.K. Sen, *Mater. Lett.*, 2002, **57**, 742-746.

[10] P. Kadam, C. Agashe and S. Mahamuni, *J. Appl. Phys*, 2008, **104**, 103501.

[11] N. Srinatha, Y. S. No, V. B. Kamble, S. Chakravarty, N. Suriyamurthy, B. Angadi, A. M. Umarji and W. K. Choi, *RSC Adv.*, 2016, **6**, 9779-9788.

[12] E. P. da Silva, M. Chaves, S. F. Durrant, P. N. Lisboa-Filho and J. R. R. Bortoleto, *Mater. Res.*, 2014, **17**, 1384-1390.

[13] L. Lu, H. Shen, H. U. I. Zhang, F. Jiang, B. Li and L. Lin, *Optoelectron. Adv. Mater.*, 2010, **4**, 596-600.

[14] M. Chaves, R. Ramos, E. Martins, E. C.Rangel, N. C. da Cruz, S. F. Durrant and J. R. R. Bortoleto, *Mater. Res.*, 2019, **22**, e20180665.

[15] V. Şenay, *J. Mater. Sci.: Mater. Electronics*, 2019, **30**, 01329.

[16] H. Kong, P. Yang and J. Chu, *J. Phys. Conf.*, 2011, **276**, 012170.

[17] M. Caglar, S. Ilican, Y. Caglar and F. Yakuphanoglu, *J. Mater. Sci. Mater. Electron.*, 2008, **19**, 704-708.

[18] J. Cho, S. Hwang, D. Ko and S. Chung, *Materials*, 2019, **12**, 3423.

[19] O. Karzazi, L. Soussi, A. Louardi, A. El Bachiri, M. Khaidar, M. Monkade, H. Erguig, M. Taleb, *Superlattices Microstruct.*, 2019, **127**, 0749-6036.

[20] G. Kaur, A. Mitra and K. L. Yadav, *Prog. Nat. Sci. Mater. Int.*, 2015, **25**, 12-21.

[21] L. Ma, X. Ai and H. Quan, *J. Korean Phys. Soc.*, 2019, **74**, 806.

[22] Z. Wang, C. Luo W. Anwand, A. Wagner, M. Butterling, M. A. Rahman, M. R. Phillips, C. Ton-That, M. Younas, S. Su and F. C. Ling. *Sci. Rep.*, 2019, **9**, 3534.

[23] S. Venkatachalam, Y. Iida, and Y. Kanno, *Superlattices Microstruct.*, 2008, **44**, 127-135.

[24] C. Liu, F. He, N. Yan, S. Zang, Y. Zuo and J. Ma, *J. Wuhan Univ. Technol. Mater. Sci.*, 2016, **31**, 1235-1239.

[25] T. Minami, H. Nanto, S. Shooji and S. Takata, *Thin Solid Films*, 1984, **111**, 167-174.

[26] Y. J. Lin, M. J. Jheng and J. J. Zeng, *Appl. Surf. Sci.*, 2010, **256**, 4493-4496.

[27] E. F. Keskenler , M. Tomakin, S. Dogan, G. Turgut, S. Aydın, S. Duman and B. Gurbulaket, *J. Alloys Compd.*, 2013, **550**, 129-132.

[28] H. Sheng, S. Muthukumar, N. W. Emanetoglu and Y. Lu, *Appl. Phys. Lett.*, 2002, **80**, 2132.

[29] F. D. Auret, S. A. Goodman, M. Hayes, M. J. Legodi and H. A. van Laarhovenet, *Appl. Phys. Lett.*, 2001, **79**, 3074.

[30] Y. Polyakov, N. B. Smirnov, E. A. Kozhukhova, V. I. Vdodin, K. Ip, Y. W. Heo, D. P. Norton and S. J. Pearton, *Appl. Phys. Lett.*, 2003, **83**, 1575.

[31] U. Ozgur, Y. I. Alivov, C. Liu, A. Teke, M. A. Reshchikov, S. Dogan, V. Avrutin, S. J. Cho and H. Morkoc, *J. Appl. Phys.*, 2005, **98**, 041301.

[32] J. Koppa, R. F. Davis and R. J. Nemanich, *Appl. Phys. Lett.*, 2003, **82,** 400.

[33] N. Ohashi, J. Tanaka, T. Ohgaki, H. Haneda, M. Ozawa and T. Tsurumi, *J. Mater. Res.*, 2002, **17**, 1529.

[34] J. C. Simpson and F. Cordaro, *J. Appl. Phys.*, 1987, **63**, 1781-1988.

[35] H. Sheng, S. Muthukumar, N. W. Emanetoglu and Y. Lu, *Appl. Phys. Lett.*, 2002, **80**, 2132.

[36] H. Dondapati, K. Santiago and A. K. Pradhan, *J. Appl. Phys.*, 2013, **114**, 143506.

[37] A. Shokri and L. Dejam, *Inter. Nano Lett.*, 2019, **9**, 161-168.

[38] M. K. Pathirane, H. H. Khaligh, I. A. Goldthorpe and W. S. Wong, *Sci. Rep.*, 2017, **7**, 8916.

[39] R. N. Chauhan, N. Tiwari, R. S. Anand and J. Kumar, *RSC Adv.*, 2016, **6**, 86770-86781.

[40] A. Barhoumi, G. Leroy, L. Yang, J. Gest, H. Boughzala, B. Duponchel, S. Guermazi and J. C. Carru, *J. Appl. Phys*, 2014, **115**, 204502.

[41] S. Singh, R. S. Srinivasa and S. S. Major, *Thin Solid Films*, 2007, **515**, 8718-8722.

[42] M. Ali Yildirim and A. Ateş, *Opt. Commun.*, 2010, **283**, 1370-1377.

[43] S. Pat, R. Mohammadigharehbagh, S. Ozen, V. Şenay, H. H. Yudar and S. Korkmaz, *Vacuum*, 2017, **141**, 210-215.

[44] Z. Ghorannevis, M. T. Hosseinnejad, M. Habibi and P. Golmahdi, *J. Theory Appl. Phys.*, 2015, **9**, 33-38.

[45] H. Park, J. M. Shin, S.Y. Cha, J.W. Park, S.Y. Jeong, H. K. Pak and C. R. Cho, *J. Korean Phys. Soc.*, 2006, **49**, 584-588.

[46] N. Shih, J. Chen and Y. Jiang, *Adv. Mater. Sci. Eng.*, 2013, 401392.

[47] A. P. Roth, J. B. Webb and D. F. Williams, *Solid State Commun.*, 1981, **39**, 269-1271.

[48] J. Jia, A. Takasaki, N. Oka and Y. Shigesato, *J. Appl. Phys.*, 2012, **112**, 013718.

[49] S. Sharma, C. Periasamy and P. Chakrabarti, *Electronic Mater. Lett.*, 2015, **11(6),** 1093-1101.

[50] A. S. Nair and J. Isac, *Int. J. Soc. Relev. Concern*, 2015, **3**, 1-11.

[51] B. S. F. T. Ba, *Inter. J. Sci. Res. Publications*, 2014, **4**, 12.

[52] C. Augustine, *Digest J. Nanomater. Biostructures*, 2018, **3**, 847-856.

[53] M. A. Hassan, C. A. Hogarth, J. Maer. sci., 1998, 23, 2500-2504.

[54] Y. Gatut, Y. H. Pramono, M. Zainuri and D. Darminto, *Micro. Nano Lett.*, 2017, **12**, 787-792.
[55] A. K. Jazmati and B. Abdallah, *Mater. Res.*, 2018, **21**, 1-6.
[56] R. B. Ganesh, N. Motwani and N. B. Chaure, *AIP Conf. Proc.*, 2017, **1832**, 080054.
[57] K. Prabakar, C. Kim and C. Lee, *Cryst. Res. Technol.*, 2005, **40**, 1150-1154.
[58] J. Ghosh, R. Ghosh and P. K. Giri, *Sensors Actuators, B Chem.*, 2018, **254**, 681-689.
[59] P. U. Londhe and N. B. Chaure, *AIP Conf. Proc.*, 2011, **1349**, 717-718.
[60] P. K. Bhujbal, H. M. Pathan and N. B. Chaure, *ES Energy Environment*, 2019, **4**, 15-18.
[61] S. Sarkar, S. Patra, S. K. Bera, G. K. Paul and R. Ghosh, *Phys. E*, 2012, **46**, 1-5.
[62] S. M. Sze, Physics of Semiconductor Devices, 2nd ed. (Wiley, New York), 1981, 292.
[63] Z. Shao, X. Zhang and X.Wang, *Sci. China Phys. Mech. Astron.*, 2010, **53**, 64.
[64] G. Yuan, Z. Ye, L. Zhu, J. Huang, Q. Qian and B. Zhao, *J. Crystal Growth*, 2004, **268**, 169-173.
[65] Ş. Aydoğan, K. Çınar, H. Asıl, C. Coşkun and A. Türüt, *J. Alloys Compd.*, 2009, **476**, 913-918.
[66] L. Rajan, C. Periasamy and V. Sahula, *Perspectives Sci.*, 2016, **8**, 66-68.
[67] G. Kaur, A. MitraandK. L. Yadav, *Progress Natural Sci.: Mater. Inter.*, 2015, **25**, 12-21.
[68] L. Avril, Ph. Guaino, F. Maseri, K. Muthukaruppasamy and J. J. Pireaux, *J. Phys. Conf. Series*, 2013, **417**, 012011.